JOURNAL OF GEOPHYSICAL RESEARCH, VOL. 113, E04004, doi: 10.1029/2007JE002928, 2008

Thickness of the magnetic crust of Mars

Coerte V. Voorhies[1]

Received 16 April 2007; revised 26 September 2007; accepted 22 January 2008; published 24 April 2008.

[1] To estimate the thickness of the magnetic crust of Mars, six observational magnetic spectra are fitted with the theoretical spectrum expected from a novel, bimodal distribution of magnetic sources. Observational spectra differ, for each comes from a different map or model of variously selected and analyzed Mars Global Surveyor Magnetometer/Electron Reflectometer measurements of the vector magnetic field around Mars. The new theoretical spectrum represents fields from both compact sources and extended, laterally correlated sources on a spherical shell, so the estimated shell depth can now be doubled to obtain layer thickness. This typical magnetic crustal thickness is put at 47.8 ± 8.4 km. The extensive sources are enormous, typically 650 km across, and account for over half the magnetic energy at low degrees. There is some indication that these sources are relatively shallow, but the typical area remains about 330,000 km^2. Granted such extended sources represent magnetization of Mars' ancient crust in a core source field dominated by a reversing, areocentric paleodipole, each one arguably formed during a single polarity chron. How did such vast regions of magnetic crust form? A survey of many eligible mechanisms suggests magnetization of cooling igneous rock at minimal rates of about 1 to 0.1 km^3/a during superchrons of order 15 to 150 Ma long.

Citation: Voorhies, C. V. (2008), Thickness of the magnetic crust of Mars, *J. Geophys. Res.*, *113*, E04004, doi:10.1029/2007JE002928.

1. Introduction

[2] The Magnetometer/Electron Reflectometer (MAG/ER) experiment aboard NASA's Mars Global Surveyor (MGS) measured the vector magnetic field around Mars. The portion of the field originating within Mars is interpreted as being of primarily crustal or lithospheric origin. Indeed, the main source of the intrinsic magnetic field of Mars is widely held to be magnetization in an ancient crust, thermoremanent magnetization (TRM) acquired in the field from a now extinct core dynamo [*Acuña et al.*, 1999, 2001].

[3] Support for this interpretation comes from regional magnetization models that closely fit strong magnetic fields measured above portions of Mars' heavily cratered, apparently ancient, southern highlands [*Connerney et al.*, 1999]. Further support comes from the ability of regional crustal demagnetization by giant impacts to explain the relatively weak fields measured over Hellas, Argyre and Isidis basins, and arguably over much of the northern lowlands [*Acuña et al.*, 1999, 2001; *Connerney et al.*, 2001, 2005; *Arkani-Hamed*, 2001b]. Global support comes from the ability of a shell of dipolar sources situated near Mars' surface to closely fit planet-wide MGS data gathered during Aero-Braking phases (AB), Science Phasing Orbits (SPO), and now Mapping Orbits (MO) [*Purucker et al.*, 2000; *Langlais et al.*, 2004].

[4] The earlier conjecture that Mars has crustal magnetization that is a thermal remanent of the field generated by a past core dynamo [*Curtis and Ness*, 1988] is supported by a clustering of paleopole position estimates [*Hood and Zakharian*, 2001; *Arkani-Hamed*, 2001a, 2002a; *Richmond and Hood*, 2002]. Such clustering is consistent with a largely dipolar, core source paleofield that occasionally reversed polarity. If an areocentric paleodipole is presumed axial to complete a terrestrial analog, then these estimates indicate appreciable polar wander. *Hood et al.* [2005] describe further indications of polar reorientation, but remote paleopole position estimates depend strongly upon how magnetic features are modeled [*Frawley and Taylor*, 2004]. Work by *Ravat* [2006] and others raise more doubts about such paleopole positions, especially from complex magnetic provinces.

[5] Pursuit of the impact shock demagnetization hypothesis led *Nimmo and Gilmore* [2001] to estimate a paleothickness for the magnetic layer of 10–100 km. It also led to identification of titanohematite [*Kletetschka et al.*, 2002] and pyrrhotite [*Hood et al.*, 2003; *Rochette et al.*, 2003], in addition to magnetite [*Kletetschka et al.*, 2000] and hematite [*Dunlop and Kletetschka*, 2001], as possible major mineral carriers of the TRM [also see *Artemieva et al.*, 2005].

[6] Mars now lacks a large-scale global field akin to Earth's but has small-scale regional magnetic features reminiscent of intense terrestrial magnetic anomalies. Physically, a close fit to the measured field thus requires either

[1]Planetary Geodynamics Laboratory, Goddard Space Flight Center, Greenbelt, Maryland, USA.

(1) an implausibly strong, small-scale, nondipolar, present-day dynamo field atop Mars' core; (2) implausibly strong magnetization deep in Mars' mantle, at temperatures that may still exceed the Curie point of planet-forming minerals; or (3) intense magnetization of Mars' cooling, thickening crust, initially by the field from a now extinct core dynamo. It is easy enough to choose 3 (see Appendix A), yet more compelling evidence for crustal sources of the intrinsic field comes from analysis of the magnetic spectrum of Mars.

[7] The spectral method for distinguishing crustal from core source magnetic fields was reexamined, modified and applied to Earth and Mars by *Voorhies et al.* [2002, hereafter referred to as paper 1]. The available observational spectrum for Mars showed only a crustal source field. It was fairly well fitted by the spectrum expected from random dipolar sources scattered on a spherical shell about 46 ± 10 km below Mars' 3389.5 km mean radius. This decorrelation depth tends to overestimate the typical depth of extended magnetized structures, and so was judged closer to source layer thickness than twice its value, even though source shell depth is usually doubled to obtain the thickness of a layer with a roughly uniform vertical distribution of magnetization.

[8] To better estimate magnetic crustal thickness, six observational magnetic spectra are here fitted with the theoretical spectrum expected from a novel, bimodal distribution of magnetic sources. The new theoretical spectrum, presented in section 3, represents fields from both compact sources and extended, laterally correlated sources. This means the estimated source depth can now be doubled to obtain a source layer thickness. The method used to solve the thorny nonlinear inverse problem posed by fitting theoretical to observational spectra is described in section 4. Observational spectra differ because each comes from a different published map or model of variously selected and analyzed MGS/MAGER measurements, as discussed in section 5. The results, estimates of source amplitude, breadth and depth, are given and discussed in section 6. Summary results are compared with other values for crustal thickness and source size, and used to draw guarded inferences about possible origins of Mars' magnetic crust, in section 7.

2. Magnetic Spectra

[9] Consider solenoidal magnetic induction $\mathbf{B}(\mathbf{r}, t)$ at position $\mathbf{r}$ and time t due to magnetization and electric current inside a planet. Outside the planet, this is the potential field $\mathbf{B} = -\nabla V$. The scalar potential V satisfies Laplace's equation, and has a spherical harmonic expansion in planet-centered spherical polar coordinates (radius r, colatitude θ, east longitude φ). Orthogonal basis functions in this expansion are products of Schmidt-normalized associated Legendre polynomials $P_n^m(\cos\theta)$ of degree n and order $m \leq n$ with circular harmonic functions of $m\varphi$ [e.g., *Langel*, 1987]. Gauss coefficients of this expansion are denoted $[g_n^m(t), h_n^m(t)]$ on the reference sphere of radius a. At larger radii, each term is attenuated by $(a/r)^{n+1}$ such that

$$V(\mathbf{r}, t) = a\sum_{n=1}^{\infty}(a/r)^{n+1}\sum_{m=0}^{n}\left[g_n^m\cos m\varphi + h_n^m\sin m\varphi\right]P_n^m(\cos\theta). \quad (1)$$

[10] A finite number of Gauss coefficients can be estimated by fitting a truncated model expansion to measured data [e.g., *Cain et al.*, 1989, 2003; *Sabaka et al.*, 2004]. Coefficients can also be calculated via numerical integrations over a field computed from an alternative representation of magnetic data, be it a map of binned measurements or an equivalent source magnetization model. Sets of coefficients obtained from different maps or models, which are derived from different data selections using different techniques, can and do differ somewhat. Such differences can be understood in light of the various methods.

[11] As is also well known, the mean square induction represented by harmonics of degree n, averaged over a sphere of radius r containing the sources, is given by [*Mauersberger*, 1956; *Lowes*, 1966; *Langel and Estes*, 1982; paper 1]

$$R_n(r) = (n+1)(a/r)^{2n+4}\sum_{m=0}^{n}\left[\left(g_n^m\right)^2+\left(h_n^m\right)^2\right]. \quad (2)$$

Quantities $2\pi r^2 R_n/\mu_0$ form a discrete magnetic spatial power spectrum for the planet at radius r, where μ_0 denotes the vacuum magnetic permeability. The R_n are here called the magnetic spectrum of the planet. At a fixed $r > a$, attenuation is exponential with n, so $\log(R_n)$ are often analyzed instead of R_n. A spectrum can be computed from any set of coefficients, so care is needed to distinguish between observational, damped, and theoretical spectra.

2.1. Observational Spectra

[12] Observational spectra can be calculated from coefficients obtained via harmonic analysis of either measured data [*Cain et al.*, 2003], binned data [*Arkani-Hamed*, 2002b, 2004], maps of binned data [*Connerney et al.*, 2001], or even fields from equivalent source models fitted to such data [*Purucker et al.*, 2000; *Langlais et al.*, 2004]. Parameterization and technique influence results, but numerical values of estimated parameters are determined by the data alone. No other information is used, so an observational spectrum cannot be obtained without observations.

2.2. Damped Spectra

[13] Damped spectra come from a model or map constrained to do something besides fitting measurements. The constraint, often a regularization hypothesis imposed via damped least squares, typically provides numerical values for parameters in the absence of any measured data. For example, continuous magnetization models by *Whaler and Purucker* [2005] were constrained to minimize the integrated square magnetization in a spherical annulus. In the absence of any observations this yields an annulus of zero magnetization. Not unknown magnetization, not indeterminate magnetization, but zero magnetization, hence zero field and zero spectrum. The constraint biases the spectrum (toward zero in this case), so damped spectra are not used here.

[14] In contrast, equivalent source models by *Purucker et al.* [2000] and *Langlais et al.* [2004] are not constrained to have weak sources. A finite number of equally spaced discrete dipoles, each representing a magnetized block, are positioned on a sphere. Dipole moments are estimated by conjugate gradient fitting of their collectively implied field

to binned measurements alone. Numerical integrations over this implied model field give coefficients needed to calculate an observational spectrum. Without measured data, block dipole moments could not be estimated, a model field could not be produced for analysis, and no spectrum could be obtained.

2.3. Theoretical Spectra

[15] Theoretical spectra are mathematical functions derived from statistical hypotheses about the sources of a magnetic field. Denoted as expectation values $\{R_n\}$, they typically have but few parameters to be estimated by fitting an observational spectrum. Evidently, the hypotheses underlying a useful theoretical spectrum, though too simple, encapsulate and inject just enough essential geophysics to enable robust estimation of key source properties, properties which could not otherwise be determined even from complete and perfect potential field data. If a theoretical spectrum were used to constrain an analysis of magnetic data, however, the result would be a constrained model from which a damped, but not an observational, spectrum could be calculated.

[16] In paper 1, the underlying hypothesis was that the spectrum could be approximated by that from myriad small, independent, magnetized geologic structures scattered on a roughly spherical shell. That injects enough geophysics to estimate the radius, hence depth, of that shell. Here that hypothesis is relaxed so as to also allow for extended source regions. This enables estimation of a source shell depth which better represents the middepth of a thin magnetic crust containing both compact and extended sources.

3. Theoretical Spectra

[17] As in paper 1, consider a thin planetary crust with compact sources. These sources may be individual rock magnetic domains or, for satellite magnetic data analysis, magnetized geologic structures up to a few tens of kilometers across. Above the planet, induction due to a large number of such compact sources can be approximated by the sum of fields from point dipoles of vector moments $\mathbf{m}^k \equiv \mathbf{M}^k/\mu_0$ at source positions $\mathbf{r}^k$ (k = 1, 2, 3, ... K). For sources scattered at random on a shell of radius r_x, positions amount to random samples from a laterally uniform distribution and are expected to be uncorrelated: $\{\mathbf{r}^k \cdot \mathbf{r}^{k'}\} = r_x^2 \delta_{kk'}$, where $\delta_{kk'}$ is the Kroenecker delta. For randomly oriented sources, we expect zero mean moment: $\{M_i^k\} = 0$, where M_i^k denotes the ith vector component of $\mathbf{M}^k$. For laterally uncorrelated sources, we expect diagonal covariance: $\{M_i^k M_{i'}^{k'}\} = \delta_{ii'}\delta_{kk'}\{M^2\}/3$, where $\{M^2\}$ is the mean square moment of the K sources in $(\mathrm{Tm}^3)^2$. The expectation spectrum from such random dipoles on a spherical shell is given by

$$\{R_n(r)\}^{ss} = A_x n(n+1/2)(n+1)(r_x/a)^{2n-2}(a/r)^{2n+4}, \qquad (3a)$$

where amplitude $A_x \equiv (2/3)K\{M^2\}/(4\pi a^3)^2$ [*Voorhies*, 1998; paper 1]. The mathematical derivation of spectrum (3a) is analogous to that of the spectrum for magnetic change induced by compact hydromagnetic eddies at the top of a fluid conductor [*Voorhies*, 2004, Appendix C].

[18] For purely radial vector moments of uncorrelated sign, upward orientations are as likely as downward ones. The expectation spectrum from such random vertical dipoles on a sphere is

$$\{R_n(r)\}^{rvd} = A_v n^2(n+1)(r_x/a)^{2n-2}(a/r)^{2n+4}, \qquad (3b)$$

where amplitude $A_v \equiv K\{M^2\}/(4\pi a^3)^2 = 3A_x/2$. When a is the planet's mean radius, then the shell depth $a - r_x$ from spectrum (3b) is also-called the decorrelation depth, but is denoted D_d.

[19] Unlike its amplitude as a function of $\{M^2\}$, the shape of a spectrum expected from an ensemble of independent sources depends very weakly upon whether individual source orientations are (1) totally random, (2) of random vertical signs, (3) of random polarities, or (4) of random directions within the local horizontal plane. For example, the ratio of spectrum (3b) to (3a) is directly proportional to $n/(n + 1/2)$. This factor deviates from unity by 1% at degree 50. The deviation is less than the differences between observational spectra for Mars and has no significant effect on numerical results for r_x presented here. Indeed, depth estimates change by less than 1 km when the spectrum from randomly oriented sources (3a) is replaced with that from random vertical sources (3b). Moreover, the ratio of spectrum (3b) to that from random polarity sources aligned by a reversing, planet centered, dipolar main field is directly proportional to $n/(n + 1/5)$, which amounts to a similarly unimportant 0.4% deviation at degree 50. Here it is enough to use random vertical sources to estimate source radius and amplitude. Rather than interpreting amplitude in terms of $\{M^2\}$, however, amplitude estimates are compared via ratios.

[20] Paper 1 gives estimates of A_x and r_x from fits of the logarithm of spectrum (3a) to log-observational spectra. For Earth we found fields from both a core of radius 3512 ± 64 km and a crust of random dipolar sources with a decorrelation depth of 4 ± 14 km. For Mars we found only a crustal source field with a decorrelation depth of 46 ± 10 km, but with sources 9.6 ± 3.2 times stronger than Earth's. More realistic theoretical spectra, which allow for magnetic crustal thickness, oblateness, and magnetization by a planet centered dipole, were also derived and discussed, as were some spectral effects of laterally correlated sources. The latter were described via an ensemble of vertically and uniformly magnetized spherical caps.

3.1. Extended Sources

[21] Extended, laterally correlated crustal sources are of interest for several reasons. In an Earth-like core source field, each magneto-geologic province with basement rock of fairly uniform magnetic susceptibility acts as an extended region of laterally correlated induced magnetization. Second, vast areas of crust can have correlated TRM; though fields from Earth's narrow seafloor stripes tend to cancel at high altitude [*Thomas*, 1987, also personal communication, 1984], broad polarity chrons do appear in satellite altitude anomaly maps, notably the Cretaceous Quiet Zones [*LaBrecque and Raymond*, 1985; *Purucker and Dymet*, 2000]. For Mars, correlated TRM in regions that cooled during like polarity intervals of an ancient core dynamo was anticipated; though many regions have evidently been demagnetized by impacts and other processes, some

extended sources survive. Third, the nonzero extent of source regions can make a planetary magnetic spectrum approach a plain exponential at harmonic degrees high enough to resolve the smallest sources, as shown in paper 1. Finally, decorrelation depth tends to overestimate the true depth of extended sources. To better estimate true source depth, we must include spectral effects of laterally extended sources. This yields an estimate we can readily interpret as the middepth of a layer with a roughly uniform vertical distribution of magnetization, hence one half the characteristic magnetic crustal thickness.

[22] Much as a crustal source field depends on the sizes, shapes, positions, orientations and total moments of magnetized geologic structures, a theoretical crustal field spectrum depends on statistical distributions for the sizes and total moments of extended sources, as well as for their shapes, orientations and patterns. Spectral effects of laterally correlated sources are explored below to improve source-depth estimates, constrain simple distribution functions, and perhaps eventually determine whether or not the different crustal magnetic dichotomies of Earth and Mars, evident in maps of the phase information, have distinct spectral signatures.

3.2. Extended Sources as Spherical Caps

[23] The basic extended source considered is again a uniform vertically magnetized cap on a sphere of planet-centered radius r_x. The cap has conical half angle ψ, with $\psi < \pi$ in the absence of magnetic monopoles, area $A = 2\pi r_x^2(1 - \cos\psi)$, total moment T, and homogeneous radial sheet magnetization S/μ_0, where sheet moment density $S = T/A$. The spectrum from one such vertically magnetized spherical cap is given by

$$[R_n(r;\psi,T)]^{\mathrm{VMSC}} = \left(T/4\pi r^3\right)^2 (r_x/r)^{2n-2}(n/2)[Z_n(\psi)]^2, \quad (4a)$$

where $Z_n = \sin\psi\ P_n^1(\cos\psi)/[1 - \cos\psi]$ [paper 1, equation (10)]. Equivalently,

$$[R_n(r;\psi,S)]^{\mathrm{VMSC}} = \left(Sr_x^2/2r^3\right)^2 (r_x/r)^{2n-2}(n/2)\left[\sin\psi P_n^1(\cos\psi)\right]^2. \quad (4b)$$

[24] Laterally isotropic caps are selected to avoid spectral effects of regionally biased magnetic fabrics that may well cancel on a planetary scale. They also have fewer geometric parameters to determine than any other shape. The field well above a variety of extended source bodies can be closely approximated using many such caps by adjusting their number, positions, sizes and total moments. This also holds for anisotropic alternatives (e.g., magnetized spherical triangles, rectangles, or ovals), however, so the selection in no way implies that the main source regions are more akin to disc-like solids than alternating polarity stripes.

[25] The selection of cap spectrum (4a) as a representative for extended sources also in no way implies that the main source regions must all be vertically magnetized. Indeed, remanent crustal magnetization will surely not be radially upward or downward everywhere on a planet. True polar wander, crustal reorientation, alteration, and Curie isotherm propagation will not conspire to zero out all remanent inclination, so a detailed physical model of remanent magnetization ought not be purely radial. As noted in section 2, however, the shape of an expectation spectrum depends very weakly upon whether independent source orientations are (1) totally random, (2) of random vertical signs, (3) of random polarities, or (4) of random directions within the local horizontal plane. This is true for compact sources, which are the limit of magnetized caps as their half angle vanishes, and so must also hold for extended caps that cover suitably modest fractions of the planetary surface.

[26] Now consider an ensemble of vertically magnetized caps on the sphere r_x with half angles ψ_k, areas $A_k = 2\pi r_x^2(1 - \cos\psi_k)$, total moments T_k of random signs, and radial sheet magnetizations S_k/μ_0 ($k = 1, 2, 3, \ldots K$). If these sources are uncorrelated, then the expected total spectrum $\{R_n(r)\}^{\mathrm{VMSC}}$ is the sum of K individual spectra, each given by equation (4a) evaluated at T_k and ψ_k. This sum can be replaced by a double integral over continuous T and ψ provided the integrand is multiplied by the sum of Dirac delta functions $\delta(T - T_k)\ \delta(\psi - \psi_k)$ and divided by K.

3.3. Cap Distribution Functions

[27] Rather than sum spectra from independent extended sources, let us define cap half angle distribution function $F(\psi)$ such that $F(\psi)d\psi$ is the number of caps with half angles in the range $[\psi,\psi + d\psi]$. Also define total moment distribution $\tau(T)$ such that $\tau(T)dT$ is the number of caps with total moments in the range $[T, T + dT]$, and sheet moment distribution $\sigma(S)$ such that $\sigma(S)dS$ is the number of caps with sheet moments in the range $[S, S + dS]$. Clearly,

$$K = \int_0^{\pi} F(\psi)d\psi = \int_{-\infty}^{\infty} \tau(T)dT = \int_{-\infty}^{\infty} \sigma(S)dS. \quad (5)$$

For solenoidal **B**, $F(\pi) = 0$; moreover, τ and σ vanish at $\pm\infty$.

[28] The size of a magnetized body does not uniquely determine its magnetic properties, nor do the latter determine the former. So neither ψ nor A uniquely determine either T or S. The spectrum expected from an ensemble of independent magnetized regions thus involves integration over a joint distribution function, hence a double integral over either ψ or A and either T or S. For a rock in a lab, measurement of dipole moment is independent of measurement of volume or area, apart from choosing the size of the apparatus. Extrinsic formulation (4a) is in this sense more fundamental, albeit perhaps less elegant, than intrinsic formulation (4b), which depends on a derived sheet moment density. In the adopted formulation,

$$\{R_n(r)\}^{\mathrm{VMSC}} = K^{-1}\left(4\pi r^3\right)^{-2}(r_x/r)^{2n-2}(n/2)\int_0^{\pi}\int_{-\infty}^{\infty} \cdot T^2\tau(T)[Z_n(\psi)]^2F(\psi)dTd\psi. \quad (6)$$

The alternative formulation in terms of $S_\sigma^2(S)$ is omitted for brevity.

[29] As an example, suppose K caps have the same size $\psi_k = \psi_0$ and uncorrelated total moments of the same magnitude $T_k = \pm T_0$. Then $F(\psi) = K\delta(\psi - \psi_0)$, $\tau(T) =$

$(K/2)\delta(|T| - |T_0|)$, and equation (6) correctly returns $\{R_n(r)\} = K(T_0/4\pi r^3)^2(r_x/r)^{2n-2}(n/2)[Z_n(\psi_0)]^2$.

[30] More generally, expectation spectrum (6) from an ensemble of independent caps is written

$$\{R_n(r)\}^{\mathrm{VMSC}} = \{T^2\}(4\pi r^3)^{-2}(r_x/r)^{2n-2}(n/2) \cdot \int_0^\pi [Z_n(\psi)]^2 F(\psi) d\psi, \quad (7)$$

where $\{T^2\}$ is the mean square total moment: the integral of $T^2\tau(T)$ over all T divided by K.

[31] Apart from the no-monopole condition $F(\pi) = 0$, there appear to be few theoretical constraints on $F(\psi)$. One may expect small sources to outnumber large ones, and so a tendency for $F(\psi)$ to decrease as ψ increases, but this does not imply monotonic $F(\psi)$. There may be a peak in $F(\psi)$ at a half angle corresponding to the typical area of magnetic provinces formed by some common geologic process. Indeed, a multimodal distribution with several peaks might better represent effects of diverse geologic and rock magnetic processes. To focus on any single such peak, one would of course introduce a characteristic half angle.

[32] In contrast, an observational spectrum for degrees 1 through N offers N constraints on weighted integrals of $F(\psi)$ via spectrum (7). To focus this information on the fewest parameters needed to describe the main spectral effect of correlated sources, size and moment distributions for extended sources are recast simply as the characteristic half angle ψ^* and the mean square total moment $\{T^2\}$ for an ensemble of vertically and uniformly magnetized spherical caps on the shell of radius r_x. The resulting expectation spectrum is

$$\{R_n(r)\}^* = \{T^2\}(4\pi r^3)^{-2}(r_x/r)^{2n-2}(n/2)[Z_n(\psi^*)]^2 = B_v(n/2)[Z_n(\psi^*)]^2(r_x/a)^{2n-2}(a/r)^{2n+4}, \quad (8)$$

where amplitude $B_v \equiv K\{T^2\}/(4\pi a^3)^2$. This would be exact if $F(\psi)$ were $K\delta(\psi - \psi^*)$.

[33] Spectrum (8) at best approximates that expected from myriad thin, independent magnetic structures of areas $A_k \approx A^* = 2\pi r_x^2(1 - \cos\psi^*)$. The approximation is arguably poorest at degrees near local minima of $[Z_n(\psi^*)]^2$; yet the larger the value of ψ^*, the lower the degree at which the first such minimum occurs. Spectrum (8) alone might thus be of some use in fitting an observational spectrum solely from very small sources through modest degree.

3.4. Small Caps

[34] In paper 1, a log-observational spectrum for Mars with $n_{\max} \le 90$ was fairly fitted with log-theoretical spectrum (3a). The latter is close to spectrum (3b), which is in turn the limit of spectrum (8) as ψ^* vanishes (recall $[Z_n(0)] = [2n(n+1)]^{1/2}$). The fair fit might suggest that contributions from small source regions dominate Mars' spectrum at these degrees, specifically, sources representable by caps with areas $A_k \ll 8\pi r_x^2/n(n+1)$, or $(1 - \cos\psi_k) \ll 4/n(n+1)$ and $\psi_k < 1.8°$ for $n < 90$. If so, coestimation of a small, but nonzero, typical cap half angle ψ^* along with B_v and r_x in spectrum (8) might reveal the typical size, amplitude, and midlayer depth for small correlated sources in Mars' magnetic crust.

[35] With $x \equiv \cos\psi_0$ and $\varepsilon \equiv 1 - x$, the finite Taylor series expansion of Z_n (paper 1, equation (11)] gives

$$Z_n(\varepsilon) = [2n(n+1)]^{1/2}[1 - (\varepsilon/4)n(n+1) + (\varepsilon^2/48)n(n+1)[n(n+1) - 2] - (\varepsilon^3/1152) \cdot n(n+1)[n(n+1) - 2][n(n+1) - 6] + \ldots]. \quad (9a)$$

For small caps $\varepsilon \ll 1$ and moderate degrees $n(n+1) \ll 4/\varepsilon$, it is enough to retain the first term in expansion (9a). To first order in $\varepsilon \approx \psi_0^2/2 \ll 4/n^2$, hence second order in ψ_0, the result is

$$Z_n^2(\psi_0 < 1/n) \approx [2n(n+1)]\left[1 - (\psi_0^2/4)n(n+1)\right]. \quad (9b)$$

Substitution of (9b) into (8) yields an approximate expectation spectrum for small spherical caps,

$$\{R_n(r)\}^{\mathrm{ssc}} = B_v n^2(n+1)\left[1 - (\psi_0^2/4)n(n+1)\right](r_x/a)^{2n-2} \cdot (a/r)^{2n+4}. \quad (10a)$$

On the reference sphere this is just

$$\{R_n(a)\}^{\mathrm{ssc}} = B_v n^2(n+1)\left[1 - (\psi_0^2/4)n(n+1)\right](r_x/a)^{2n-2}. \quad (10b)$$

Because $n\psi_0 < 1$, $\ln[1 - (\psi_0^2/4)n(n+1)]$ is about $-\psi_0^2 n(n+1)/4$ and the log of the cubically demodulated spectrum for small caps is closely approximated by

$$\ln\left[\{R_n(a)\}^{\mathrm{ssc}}/n^2(n+1)\right] = \ln(B_v) + 2(n-1)\ln(r_x/a) - (\psi_0^2/4)n(n+1). \quad (10c)$$

This is a parabola in n. The negative curvature is controlled by ψ_0^2, hence cap area $A_0 \approx \pi r_x^2 \psi_0^2$.

[36] Spectra (10a), (10b), (10c) are for small caps at moderate degrees $(n\psi_0)^2 \ll 8$. This condition means that the sources, notably cap boundaries, are not sharply resolved. The partial derivatives of the logarithm of spectrum (10b) with respect to $\ln(B_v)$, $\ln(r_x/a)$, and ψ_0 are

$$\partial \ln\{R_n(a)\}^{\mathrm{ssc}}/\partial \ln(B_v) = 1 \quad (11a)$$

$$\partial \ln\{R_n(a)\}^{\mathrm{ssc}}/\partial \ln(r_x/a) = 2n - 2 \quad (11b)$$

$$\partial \ln\{R_n(a)\}^{\mathrm{ssc}}/\partial\psi_0 = -\psi_0 n(n+1)/\left[2 - (\psi_0^2/2)n(n+1)\right]. \quad (11c)$$

Partial (11c) is approximately $-\psi_0 n(n+1)/2$, so derivatives (11a)–(11c) with respect to log amplitude, lognormalized source radius, and cap half angle are almost proportional to 1, n and $-n^2$, respectively. The negative sign here, and in equations (10a)–(10c), describes the softening of the spectrum due to the small but nonzero extent of the sources. A fit to such a softer spectrum using amplitude and source

radius alone will underestimate r_x, and hence overestimate source depth.

[37] A fit of log-demodulated small caps spectrum (10c) to a log-demodulated observational spectrum amounts to a parabolic fit in harmonic degree, as opposed to a linear fit with the log-demodulated spectrum from random vertical dipoles. Separation of a small characteristic source diameter from amplitude and depth should thus be straightforward, unlike explicit separation of amplitude from layer thickness. Yet this is not the case for Mars. Indeed, early efforts returned purely imaginary ψ_0, not because the dominant source regions have "negative areas" reflecting impact demagnetization, but because they are not small.

3.5. A Bimodal Source Distribution

[38] Consider a thin crust containing both myriad compact magnetic sources and some independent extended source regions, regions within which vertically averaged magnetization has strong positive lateral two-point correlations. The expected magnetic spectrum from such a crust is the sum of two spectra, one from compact sources, the other from extended sources. The spectrum from the compact sources is represented by spectrum (3b) for random vertical dipoles on a sphere, noting that similar functional forms are obtained from compact sources aligned by a reversing planet-centered dipole as well as of random orientation [*Voorhies*, 1998]. The spectrum from the extended sources is represented simply by spectrum (8) for vertically magnetized spherical caps of characteristic half angle ψ^* on the same sphere, now denoted r_c.

[39] The total spectrum expected from this bimodal distribution of both random compact sources and independent extended sources is the sum of spectra (3b) and (8),

$$\{R_n(r)\} = A_v n^2(n+1)\left(1 + [B_v/A_v][Z_n(\psi^*)/Z_n(0)]^2\right) \cdot (r_c/a)^{2n-2}(a/r)^{2n+4}, \tag{12a}$$

where $[Z_n(0)]^2 = 2n(n+1)$. On the reference sphere, this is just

$$\{R_n(a)\} = A_v n^2(n+1)(1 + [B_v/A_v][Z_n(\psi^*)/Z_n(0)]^2)(r_c/a)^{2n-2}, \tag{12b}$$

which yields the log cubically demodulated expectation spectrum

$$\ln\left[\{R_n(a)\}/n^2(n+1)\right] = \ln(A_v) + (2n-2)\ln(r_c/a) + \ln\left(1 + [B_v/A_v][Z_n(\psi^*)/Z_n(0)]^2\right) \tag{12c}$$

This is the new theoretical spectrum used to estimate the typical depth, $z \equiv a - r_c \neq D_d$, to both compact and extended crustal sources. More elaborate treatments introduce more parameters.

4. Method

[40] Spectral parameters are here estimated by least squares fits of log-theoretical to log-observational spectra for Mars from degree n_{min} to n_{max}. The objective function minimized is the sum of squared logarithmic residuals per degree of freedom,

$$s_P^2 = (n_{max} - n_{min} + 1 - P)^{-1} \sum_{n_{min}}^{n_{max}} (\ln[R_n(a)] - \ln\{R_n(a)\})^2, \tag{13}$$

where a = 3389.5 km and P is the number of parameters estimated (2, 3, or 4 for spectra (3b), (10b) or (12b), respectively). Because upward continuation to radius $r > a$ both adds and subtracts $(2n + 4)\ln(r/a)$ within the summed square on the right of equation (13), numerical estimates of the parameters $(\ln(A_v), \ln(r_x/a); \psi^*; A_v/B_v)$ do not depend on the altitude at which a log-observational spectrum is fitted. Similarly, log-demodulated spectra can be fitted by dividing both theoretical and observational spectra by $n^2(n + 1)$, hence subtracting and adding $\ln[n^2(n + 1)]$ within the summed square, with no change in the estimates. Misfit is also summarized by scatter factor F_P, the exponential of the root mean square logarithmic residual:

$$F_P = \exp\left(\left[s_P^2(n_{max} - n_{min} + 1 - P)/(n_{max} - n_{min} + 1)\right]^{1/2}\right) \tag{14}$$

[41] In principle, minimum s_P^2 would yield a maximum likelihood estimate if logarithmic residuals $\ln(R_n/\{R_n\})$ were normally distributed with covariance $\{\ln(R_n/\{R_n\})\ln(R_{n'}/\{R_{n'}\})\}$ equal to the identity matrix. Such a lognormal distribution can better approximate a chi-square distribution than a normal distribution [*Voorhies*, 2006]. The statistical significance of the residuals is deemed large, owing to the precision of observational spectra determined by analyses of high accuracy MGS data, and could be estimated if the inverse covariance for $\ln R_n$ were available. The a priori covariance of logarithmic residuals, hence the weight matrix, is here set to the identity matrix in anticipation of large fluctuations, a factor of $e^{\pm 1}$, about simple theoretical spectra. Linear, or iterative linearized, estimation of parameters requires computation of the expected parameter covariance; the square roots of its diagonals give expected parameter errors. Multiplication of these by s_P, which turns out to be about 0.25, yields scaled error estimates. Differences between parameters estimated by fitting different observational spectra are here considered more useful indicators of parameter uncertainty.

[42] In practice, log-observational spectra for Mars exhibit positive excess curvature for degrees 20–40. At and near $\psi^* = 0$, this makes the objective function s_4^2 increase with ψ^*, hence $(\psi^*)^2$. Again, this is not because the dominant extended sources have "negative areas", perhaps reflecting impact demagnetization, but because they are so large that small cap linearization (10a) fails, as verified by the minimum objective function at large values of ψ^*. Inclusion of higher-order terms can help solve the nonlinear inverse problem, yet with too small a trial value for ψ^*, the positive slope of the objective function near $\psi^* = 0$ leads iterative linearized solutions astray. And values of $[Z_n(\psi^*)/$

$Z_n(0)]^2$ depend strongly on ψ^*, so convergence from even a good guess of ψ^* can be slow. The nonlinearity frustrates linearized coestimation of parameters.

[43] The closest fits of spectrum (12c) to log-observational spectra are instead found by sweeping through trial values of both relative amplitude B_v/A_v and characteristic half angle ψ^* for correlated sources and, for each pair, solving the linear subsystem for optimal $\ln A_v$ and $\ln(r_c/a)^2$. Four sweeps of ever finer resolution are usually enough to locate the minimum sum of squared logarithmic residuals per degree of freedom, s_4^2, to 6 digits, and optimal B_v/A_v and ψ^* to 3.

5. Observational Spectra

[44] Six observational spectra were fitted using the method above for various degrees (n_{min}, n_{max}). The recommended degree range for each spectrum is largely dictated by published analyses of measured data. These ranges are important, reflect key points made by various authorities about their analyses, and are best understood in light of the diverse methods used to construct spherical harmonic representations, maps, or equivalent source models of measured data.

[45] The spectrum denoted FSUW90 is from the spherical harmonic analysis through degree and order $N = 90$ of measured MGS data by *Cain et al.* [2003]. About 110,000 measurements were selected to homogenize areal data density and give global coverage. A preliminary field model was fitted to these data, then used to remove spurious values and determine weights for classes of data gathered during AB1 and AB2, SPO, and MO. These weights were used in their final analysis, performed in areodetic coordinates with a reference radius of 3390 km. The resulting potential field fits nightside vertical component MO data to about 5.9 nT (1σ, -0.3 nT mean) and dayside northward component AB data to 13.5 nT (1σ, -2.4 nT mean). The resulting coefficients were used to compute spectrum FSUW90 via equation (2).

[46] *Cain et al.* [2003] point out that: most of the power in the spectrum at 145 km altitude is between degrees 15–40; the dipole power is likely close to the noise level; and the highest degree coefficients are statistically insignificant individually, yet are collectively needed to adequately model small-scale variations. These points dictate selection of R_n in the range $n_{min} > 1$ and $n_{max} = 90$ or perhaps less. To investigate effects of both high and very low degree R_n, separate fits are tried with n_{max} set to either 90 or 50, and n_{min} set to 2, 3, or 6.

[47] Many spectra were provided by J. Arkani-Hamed (personal communication, 2005). The spectrum denoted LAMGU is from a spherical harmonic analysis through degree and order 65 of binned, nightside MGS vector data by *Arkani-Hamed* [2002b]. The bins are $0.5^\circ \times 0.5^\circ$ in (θ,φ) and 10 km thick. For bins with 3 or more data, outliers over 2σ from the mean were rejected and the process repeated. About 274,000 bins had more than 1 accepted measurement; most had 10–50. *Arkani-Hamed* [2002b] describes 3 sets of 4 field models each, with sets through degree 55, 60, or 65 and models fitting either radial, radial and one horizontal component, or all three vector components. There are also separate analyses of low-altitude data (80–200 km) and high-altitude data (320–420 km). Correlations between coefficients from different models were very high only for degrees 4–50, which indicates the range $n_{min} > 3$ and $n_{max} = 50 < 65$. Comparison of spectra from low- versus high-altitude data, however, shows not only that R_1 is not very well determined, but that low-altitude data reduce R_n for $n > 50$. To investigate this, spectrum LAMGU from the low-altitude data is selected and analyzed with $n_{max} = 65$ and then 50, and with n_{min} set to 4, 5, or 6.

[48] Spectrum MGU is from the correlative spherical harmonic analysis through degree $N = 90$ of nightside MGS data by *Arkani-Hamed* [2004]. Only vertical component MO data were used. The data were separated into two sets for two separate analyses [see also *Arkani-Hamed et al.*, 1994; *Cain et al.*, 1967] and averaged in 0.5° bins. Only bins with more than one datum were used, with 2σ outlier rejection in bins with more than 3 data; about 90% of the bins kept more than 15 measured data. The two sets of Gauss coefficients have correlation coefficients greater than 0.75 through degree 60. The two spectra are, however, quite similar through degree 65. The final correlative coefficients used to calculate spectrum MGU are a kind of weighted average of the two sets: when both coefficients have the same sign, the arithmetic mean is used; when they have opposite signs, hence negative correlation, the final coefficient is set to zero. *Arkani-Hamed* [2004] selects maximum degree 62 based on correlations between coefficients; however, spectrum MGU is analyzed here with $n_{max} = 65$ and then 50, and with $n_{min} = 2$ or 3.

[49] Like damping, zeroing out poorly determined coefficients can increase misfit and yield a simpler map of a downwardly continued, internal source field. Of course, neither coefficients driven to tiny amplitudes by damping or zeroing, nor coefficients driven to excess amplitudes by fitting noise, are reliable. Neither produce a reliable spectrum. Compared with other analyses of MO data, the correlative averaging technique preferentially reduces power at higher degrees, as expected. But it is no substitute for low-altitude data as a constraint on coefficient magnitudes, hence the spectrum, above degree 65 [see *Arkani-Hamed*, 2004, Figure 7]. Indeed, low-altitude data can strongly constrain the spectrum above degree 65, and arguably above 50, where some spectra begin to deviate markedly from others.

[50] Spectrum CONN comes from the global magnetic maps of Mars by *Connerney et al.* [2001] via an analysis by J. Arkani-Hamed (personal communication, 2005). Dark hemisphere MO data were averaged along track and decimated in time to give an averaged value for each field component at every degree of latitude. These track averages were sorted into $1^\circ \times 1^\circ$ bins; the median within each bin was used to make a digital map for each component. This mapping requires no fitting, apart from taking averages and medians, so it has high fidelity. It is not a potential field analysis, however, so there is neither assumption nor assurance of either a potential or a solenoidal field. The thinness of the annulus sampled by the near circular MO provides some altitude normalization and coefficients can be obtained via harmonic analysis of the mapped radial component. When fitting observational spectrum CONN, I chose $1 < n_{min} < 5$ and $n_{max} = 50$.

[51] Spectrum P87 is from the equivalent source model of *Purucker et al.* [2000]. Amplitudes of 11,550 radial dipoles,

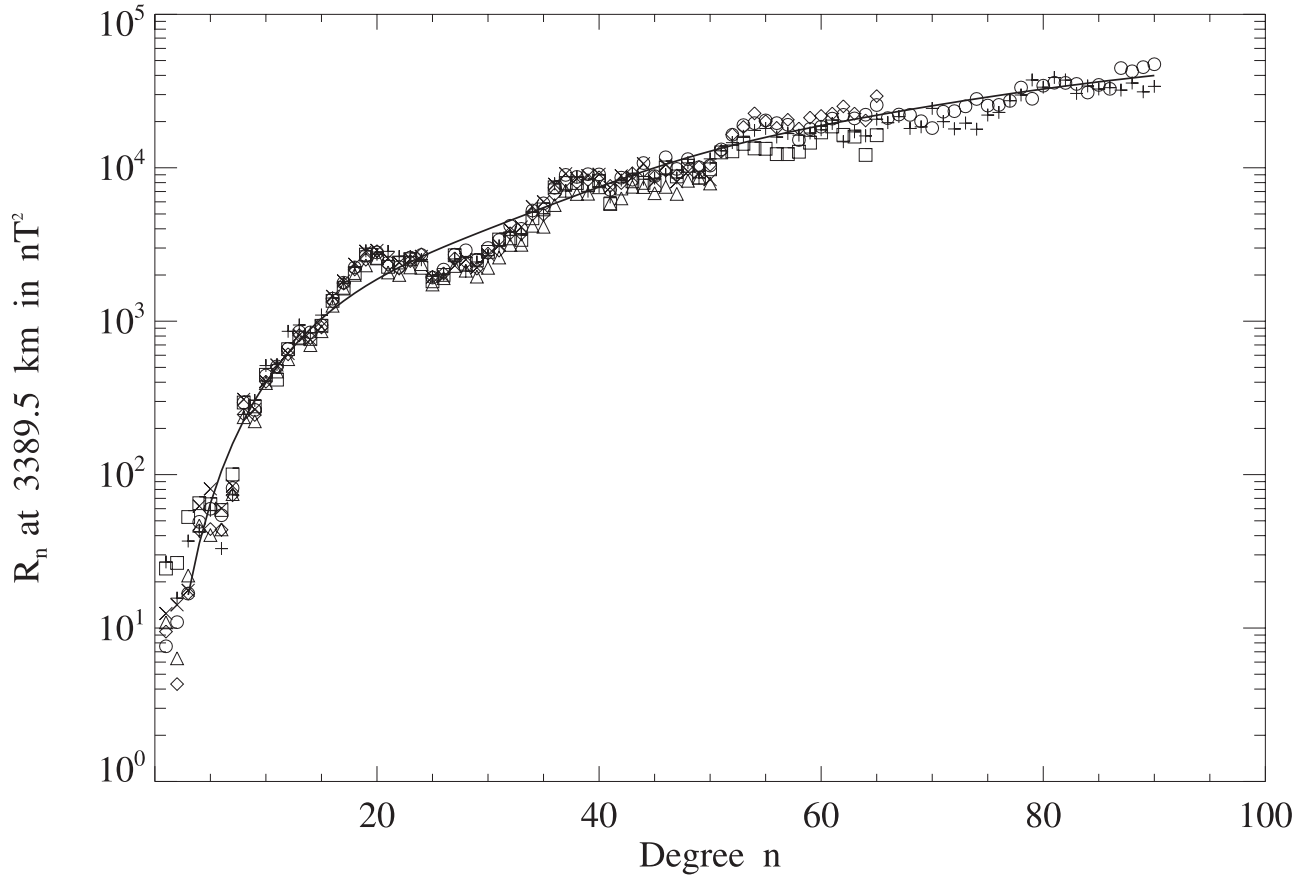

Figure 1. Observational magnetic spectra of Mars, downwardly continued to 3389.5 km radius. Spectrum FSUW90 is shown for degrees 1–90 (circles), LAMGU for degrees 1–65 (squares), MGU for degrees 1–65 (diamonds), CONN for degrees 1–50 (triangles), P87 for degrees 1–90 (pluses), and LPM for degrees 1–50 (crosses). Also shown is the best fit of the log of theoretical bimodal spectrum (12b) to the log of spectrum FSUW90 for degrees 3–90 (solid curve, see Table 1 for fit parameters).

with a 111.9 km mean spacing on the sphere of radius 3393.5 km, were fitted to binned MGS vertical component data (1° × 1° bins, 10 km thick). Numerical integrations over the implied model field were used to compute coefficients and spectrum P87, as described in paper 1. This is the spectrum for the field constructed without the 1500 km cutoff used to obtain a sparse matrix for the conjugate gradient method. Spectrum P87 is analyzed with $n_{min} = 6$ and n_{max} set to either 90 or 76 for reasons given in paper 1.

[52] Spectrum LPM is from an equivalent source model by *Langlais et al.* [2004]. They separated MAG/ER data into two sets: a low-altitude set from AB1, SPO, and AB2 (below 350 km), and a high-altitude set from 1999 MO data (370–430 km). Only nighttime SPO and MO data were selected, but dayside AB data were retained. Outliers relative to the model by *Purucker et al.* [2000] were rejected (50 nT for AB and SPO data, 9 nT for MO). The data were binned into 1° × 1° blocks, 10 km thick, and mean values computed for each bin: l03,996 at low altitudes, 75,380 at high altitude. Various data subsets were used to estimate amplitudes and directions of dipoles at tessellated icosahedral mesh points on a sphere via a conjugate gradient technique. The spectrum used here is from their preferred model, M23/-20/14, with 4840 vector dipoles at radius 3373.5 km and a mean spacing of about 173 km. Residuals relative to the MO data set are but 3.3 nT RMS in B_r. Residuals at lower altitudes are larger not only due to external source fields in dayside AB data, but because the source spacing makes it difficult to fit data below 200 km. *Langlais et al.* [2004] state that any conclusions drawn from the spectrum of their model for n higher than 50 would be hazardous. Therefore, $n_{max} = 50$ for spectrum LPM. Empirically, inclusion of R_1 causes a markedly larger misfit to all spectra studied; for LPM, I further chose $n_{min} > 2$ to keep $s_P^2 < 10\%$. B. Langlais (personal communication, 2007) points out that n_{min} should again be 6 because the 1500 km cutoff was again used to form a tractably sparse matrix.

[53] Figure 1 shows the six observational spectra downward continued to radius $a = 3389.5$ km and the 4 parameter best fit of the log of bimodal spectrum (12b) to the log of spectrum FSUW90 for degrees 3–90 (solid curve). Though obtained by different groups using different methods to analyze different MGS data selections, the agreement between observational spectra is remarkable. The symbols cluster especially tightly for degrees 7–50. Local spectral maxima above the solid curve near degrees 19 and 38, and local minima below it near degrees 25–30 and 50, create an undulating, wave-like appearance. Considerable scatter at degrees 1–3 is unsurprising in light of points made by various authors. For degrees 50–65, MGU (diamonds)

Table 1. Results of Magneto-Spectral Analyses Within Recommended Ranges of Degree n[a]

Spectrum	n	D_d (km)	s_2^2 (%)	s_4^2 (%)	F_4	B_v/A_v	ψ^* (deg)	z (km)	Unscaled Error	z/D_d	$\pm1\sigma$ Test?
FSUW90	2–90	40.1	7.83	4.84	1.24	1.48	5.78	25.5	6.9	0.64	Yes
FSUW90	3–90	38.8	6.83	4.42	1.23	1.33	5.57	25.4	7.1	0.65	Yes
FSUW90	6–90	37.1	6.28	4.43	1.23	1.24	5.46	25.4	7.4	0.68	Yes
FSUW90	2–50	62.3	8.36	7.48	1.30	1.51	5.85	26.3	17.0	0.42	Yes
FSUW90	3–50	59.3	7.48	6.73	1.28	1.67	5.49	19.4	17.6	0.33	Yes
LAMGU	4–65	55.5	7.35	5.44	1.25	1.43	5.84	32.8	11.9	0.59	No
LAMGU	6–65	52.8	6.44	5.06	1.24	1.27	5.58	32.5	12.5	0.62	No
LAMGU	4–50	66.6	7.81	6.75	1.28	1.72	5.75	23.3	18.1	0.35	Yes
LAMGU	5–50	63.5	6.93	6.07	1.27	1.89	5.36	20.2	18.7	0.32	Yes
MGU	2–65	41.1	9.37	6.10	1.27	2.37	5.29	5.7	11.4	0.14	No
MGU	3–65	40.9	9.52	6.19	1.27	2.38	5.33	6.0	11.7	0.15	No
MGU	2–50	57.4	8.30	7.55	1.30	2.29	5.19	7.2	17.1	0.13	No
MGU	3–50	57.8	8.46	7.69	1.30	2.20	5.23	9.0	17.6	0.16	No
CONN	2–50	68.6	8.88	8.09	1.31	1.91	5.46	24.7	17.0	0.36	Yes
CONN	3–50	67.6	8.93	8.17	1.31	2.03	5.35	21.7	17.5	0.32	Yes
CONN	4–50	65.5	8.66	7.91	1.31	2.35	5.13	14.5	18.2	0.22	Yes
P87	6–90	39.8	9.00	6.58	1.28	1.55	5.32	25.6	7.4	0.64	Yes
P87	6–76	46.5	8.93	7.49	1.30	1.26	5.31	30.1	9.7	0.65	Yes
LPM	3–50	65.1	9.46	8.86	1.33	1.29	5.96	33.3	17.5	0.51	No
LPM	6–50	60.4	9.00	8.77	1.33	1.23	5.44	29.1	19.3	0.48	Yes
20-point means		54.3				1.72	5.48	21.9		0.40	Mixed
SD		±11.2				±0.42	±0.24	±9.0			
13-point means		55.1				1.63	5.48	23.9		0.43	Yes
SD		±12.5				±0.34	±0.21	±4.2			

[a]The spectrum fitted and degree range $n_{min} - n_{max}$; decorrelation depth D_d and misfit s_2^2 from two parameter fit; and from four-parameter fit with the bimodal spectrum, misfit s_4^2, scatter factor F_4, ratio of extended-to-compact source amplitudes B_v/A_v, half angle of extended sources ψ^*, source depth z, unscaled error in z (about 4 times formal error), ratio z/D_d, and whether or not z is within ± 1σ of 20 point mean. SD, standard deviation.

tends to have more power than other spectra (as expected without low-altitude data constraints) and LAMGU (squares) tends to have less power (perhaps because of less MO data coverage). The agreement between spectra FSUW90 (circles) and P87 (plusses), obtained by vastly different methods, is perhaps most clearly visible at degrees 65–90.

[54] Some figures found elsewhere show spectra which, for $n > 50$, lie either far above or far below those in Figure 1 [see, e.g., *Arkani-Hamed*, 2004, Figure 7; *Whaler and Purucker*, 2005, Figure 5; *Chiao et al.*, 2006, Figure 9]. Those far above tend to be unconstrained by low-altitude data and have invariably been carried to degrees higher than recommended; some of those far below have too. The rest are damped spectra biased by otherwise well-intentioned model norms.

6. Results

[55] Most, but not all, fits of theoretical spectra (3b) and (12a) to observational spectra relied solely upon R_n at degrees within the ranges established in section 5. Those which do are presented and discussed before summarizing lessons from those which do not.

6.1. Results From Recommended Degree Ranges

[56] Table 1 shows the results of fitting log-theoretical to log-observational spectra for various ranges of degree within those indicated above. The first column identifies the observational spectrum fitted; the second gives the range of degrees n fitted. Columns three and four list results from fits with the two parameter, random vertical dipoles spectrum (3b): decorrelation depth D_d in km below 3389.5 km and misfit s_2^2 in percent from equation (13). The remaining columns list results from fits with the four parameter, bimodal spectrum (12a). Column five gives the misfit s_4^2 in percent from equation (13). Comparison of column five with four shows that in every case $s_4^2 < s_2^2$. Because s_P^2 is the sum of squared logarithmic residuals per degree of freedom, this means that inclusion of laterally correlated sources both tightens and improves the fit. Evidently, vast regions of Mars' crust are indeed coherently magnetized.

[57] Columns six, seven and eight of Table 1 give the scatter factor F_4 from equation (14), the ratio of extensive to compact source amplitudes B_v/A_v, and the characteristic half angle of laterally correlated sources ψ^* in degrees, respectively. Column nine gives the source shell depth z below 3389.5 km. Column ten gives the absolute value of the unscaled error in z from the subfit at fixed (B_v/A_v, ψ^*); multiplication of this by s_4, a factor between 0.21 and 0.29, gives scaled error at optimal (B_v/A_v, ψ^*). Column eleven gives the ratio z/D_d.

[58] Table 1 also lists the 20 point arithmetic means and standard deviations of the estimated parameters. Seven of 20 tabulated depths z fall outside the $\pm1\sigma$ range. Outliers were rejected in the underlying MGS-MAG/ER data analyses, so column twelve answers the question: does the value of z pass the $\pm1\sigma$ outlier test? The bottom lines of Table 1 give the means and standard deviations of parameters estimated from the 13 magneto-spectral analyses which pass this test.

6.2. Discussion

[59] Decorrelation depths D_d in Table 1 are all positive, range from 37 to 69 km, and average to 54 km. Small changes in $n_{min} > 1$ produce only small changes in D_d and other parameters. When n_{max} is cut to 50, however, D_d from FSUW90, LAMGU and MGU deepen and approach values

from CONN and LPM. This is not because the spectrum of Mars increases more rapidly with degree for $n < 50$ than it does for $n > 50$, as is evident in Figure 1. It is because the slope of the log cubically demodulated spectrum becomes less negative at higher degrees. This decrease of D_d as n_{max} increases is also found in P87. It does not necessarily imply that narrower-scale sources are shallower because it is also expected from laterally correlated sources, which have a modulation factor softer than a cubic at degrees high enough to begin resolving their extent. Truncation of n_{max} to 50 increases the misfit s_2^2 of spectrum (3b) to FSUW90 and LAMGU, which are constrained by low-altitude data, but decreases s_2^2 from MGU, which runs a bit above other spectra for $n > 50$ (see diamonds in Figure 1).

[60] When fitted with bimodal spectrum (12a), however, the values of s_4^2 in Table 1 show these three spectra are all better fitted when n_{max} is not cut to 50. The main residuals are from the undulation in the spectrum from degree 17 to 33, so truncation of n_{max} to 50 reduces the degrees of freedom more than the sum of squared residuals. The better fits and modest changes in parameters (B_v/A_v, ψ^*, z) found when n_{max} is not cut arguably indicate that some analyses of MGS-MAG/ER data, notably those including low-altitude data, reliably determine observational spectrum (2) to degree 90 or so, even though some coefficients may be poorly determined.

[61] Random coefficient errors may come from sparse coverage at low altitude as well as fluctuating external fields. Unlike systematic damping, random errors in the coefficients cause partially canceling errors in the sum of their squares, hence R_n. Specifically, random errors ($\pm\varepsilon_n^m$, $\pm\delta_n^m$) in (g_n^m, h_n^m) enjoy $\{\pm 2\varepsilon_n^m g_n^m\} = 0$, so $\{(g_n^m \pm \varepsilon_n^m)^2\} = \{(g_n^m)^2\} + \{(\varepsilon_n^m)^2\}$ and random errors of ±100% in high degree coefficients, which wreak havoc on a downward continued magnetic map, typically increase R_n only by a factor of $2 < e$. The spectrum may thus be reliably determined to a higher degree than the phase information sought for global maps.

[62] The fact remains that $s_4^2 < s_2^2$ in all cases, so inclusion of laterally correlated sources improves the fit. The improvement is modest because the undulation is not well fitted. Still better fits might be obtained with multimodal cap distribution functions, possibly with different typical source depths for different modes. The phase information shows strong fields confined to one magnetic province (see section 7.2), however, so positions, sizes and amplitudes of the extended sources themselves might have to be correlated to properly fit the undulation.

[63] The scatter factors F_4 in Table 1 are at most 1.33. The best fit to any single observational spectrum analyzed is that of bimodal spectrum (12b) to FSUW90 for degrees 3 through 90. This is shown as the solid curve in Figure 1. It gives $s_4^2 = 4.42\%$ and $F_4 = 1.23$, so these R_n are typically fitted to within a factor of $(1.23)^{\pm 1}$, or roughly ±21%.

[64] Amplitude ratios B_v/A_v in Table 1 all exceed unity, so magnetized caps contribute more to the low degree part of the spectrum than do compact sources. The ratios range from 1.23 to 2.38. Ratios from MGU and CONN are somewhat larger than from other spectra. These are the two spectra from MO data alone. Because higher degree, narrower-scale fields from the crust are more attenuated at the higher MO altitudes, attenuated sensitivity to narrow-scale fields from compact crustal sources may arguably help explain these larger amplitude ratios.

[65] Values of characteristic cap half angle ψ^* in Table 1 are tightly clustered between 5° and 6° and average to 5.48°. The corresponding correlated source regions are typically about 650 km across and have areas of about 330,000 km^2, about the size of the State of New Mexico.

[66] The 20 bimodal source shell depths z in Table 1 are also all positive, range from 5.7 to 33.3 km, and average to 21.9 ± 9.0 km (±1σ). Values from MGU are shallower than those from other spectra, even from CONN. It can be argued that use of both MO data alone and correlative averaging accentuates fields from extended sources at the expense of fields from compact sources. The larger B_v/A_v ratio from MGU support this argument. The shallow values of z from spectrum MGU thus arguably offer an indication that vast, New Mexico size, regions of correlated magnetization in Mars might be shallower than more compact sources.

[67] The 20 absolute unscaled errors in z from Table 1 average to 14.1 km, which exceeds the 9.0 km standard deviation, and are quite large when n_{max} is only 50. They are far larger than the absolute scaled errors (not shown), which range from 1.5 km to 5.7 km and average to 3.7 km. Scaled errors are too small because they come from the subcovariance at optimal (B_v/A_v, ψ^*); moreover, spectrum (12a) is too simple to treat them as formal errors on a complete model. Because unscaled errors are too large and scaled errors are too small, the ±1σ outlier test is used to estimate parameter uncertainties without significantly altering the means. Normally, 13 or 14 (68% of) values for z would pass this test; 13 do. The 13 point means values and uncertainties from Table 1 put typical source depth at z = 23.9 ± 4.2 km, amplitude ratio at $B_v/A_v = 1.63 \pm 0.34$, and half width of correlated sources at $\psi^* = 5.48 \pm 0.21°$. The typical thickness of Mars' magnetic crust is put at $2z$ = 47.8 ± 8.4 km.

[68] Depth ratios z/D_d in Table 1 average to about 0.4. Decorrelation depth overestimates typical source depth by a factor of about 2 or more, and is indeed a better measure of source layer thickness than of source depth. Depth ratios from MGU are considerably less than average. Again, it can be argued that correlative averaging of two sets of coefficients from MO data analyses enhances broad-scale features from correlated sources, yet filters out narrow-scale fields from compact crustal sources, fields evident, albeit perhaps undersampled, in low-altitude data.

6.3. Lessons From Other Degrees

[69] Table 2 has the same format as Table 1, but lists quantities obtained by fitting spectra outside the degree ranges established in section 5. Though $s_4^2 < s_2^2$ as before, s_2^2 now exceeds 10% and reaches 26%; even s_4^2 reaches 20%. The first six rows show effects of ignoring the warning by *Cain et al.* [2003] that dipole power is likely close to the noise level. Merely setting $n_{min} = 1$ doubles the misfit! Comparison of Tables 1 to 2 shows that s_4^2 jumps from about 4.5% to 9.0% for FSUW90, from 7% to 15% for truncated FSUW90, from about 7% to 19% for MGU and P87, and from 9% to 21% for LPM. So doing also increases ψ^* by about a degree, and increases both D_d and z, albeit mainly for fits with $n_{max} = 50$ (MGU, LPM).

Table 2. Effects of Going Outside Recommended Degree Ranges

Spectrum	n	D_d (km)	s_2^2 (%)	s_4^2 (%)	F_4	B_v/A_v	ψ^* (deg)	z (km)	Unscaled Error	z/D_d	$\pm1\sigma$ Test?
FSUW90	1–90	42.9	13.74	9.01	1.34	1.96	6.50	26.2	6.8	0.61	Yes
FSUW90	1–50	70.4	16.36	15.01	1.45	1.48	6.70	36.5	16.4	0.52	No
MGU	1–65	47.2	19.57	15.04	1.46	2.69	6.03	10.9	11.2	0.23	No
MGU	1–50	67.0	19.65	18.98	1.52	1.47	6.21	32.0	16.5	0.48	No
P87	1–90	48.4	26.16	18.51	1.52	2.95	6.60	26.9	6.8	0.55	Yes
LPM	1–50	78.5	22.36	20.56	1.54	1.59	7.17	44.1	16.4	0.56	No
LPM	2–50	68.9	10.91	9.98	1.35	1.35	6.33	36.6	16.9	0.53	No
LAMGU	3–50	71.8	10.54	9.01	1.33	1.72	6.31	34.1	17.5	0.47	No
LPM	6–90	91.7	13.75	6.49	1.28	41	2.25	19.2	7.4	0.21	Yes

[70] Four values for R_1 are below that from FSUW90, below the noise level indicated by *Cain et al.* [2003] (see Figure 1). Yet all six dubious values for R_1 are far larger than indicated by extrapolation of theoretical spectra fitted to higher degree R_n. In this curious sense, Mars' poorly determined dipole power seems anomalously large. This is not a true dipole anomaly, however, for the upper bound on Mars' dipole moment of 2×10^{17} A m^2 by *Acuña et al.* [2001] implies that $R_1 < 0.53$ nT^2, which is less than can be shown in Figure 1.

[71] To illustrate valid concerns about other low degree coefficients [*Arkani-Hamed*, 2002b], rows seven and eight in Table 2 show effects of including degree 2 of LPM, and degree 2 of LAMGU, respectively. The misfits are not nearly so large as with $n_{min} = 1$, yet these attempts give ψ^* over 6°, exceeding all values in Table 1. And they give values for D_d and z greater than any in Table 1, including values from fits to these spectra with slightly larger n_{min}.

[72] The bottom line of Table 2 demonstrates effects of irresponsibly fitting spectrum LPM far into the hazard zone ($n > 50$) identified by *Langlais et al.* [2004]. In this case, D_d is very large and s_2^2 is uncomfortably large, but misfit s_4^2 is fairly small and z is quite plausible. Amplitude ratio B_v/A_v, however, becomes huge and ψ^* collapses. What happened? Above degree 50, spectrum LPM lies below other observational spectra [*Langlais et al.*, 2004; *Arkani-Hamed*, 2004, Figure 7], albeit not so far below as some damped spectra [*Whaler and Purucker*, 2005, Figure 5; *Chiao et al.*, 2006, Figure 9]. A close fit to such reduced power at $n > 50$ with spectrum (12a) requires reduced amplitude for compact sources A_v, but to keep a close fit at low degrees further requires a compensating increase in extended source amplitude B_v. This inflates B_v/A_v. The implausible decrease in ψ^* stretches this compensating effect to intermediate degrees.

[73] Does this strained fit better represent real properties of either the magnetic spectrum or the magnetization of Mars? No. *Langlais et al.* [2004] point out that the source spacing of model M23/-20/14, about 173 km or 2.9°, does not allow as close a fit to low-altitude data as some other models. Evidently, the low-altitude data prevent excessive R_n above degree 50, but are not fitted closely enough for LPM to reveal the higher degree power seen in FSUW90 or P87. Moreover, a cap half angle of but 2.25° (133 km radius) is less than the source spacing. Such a cap does not quite cover the area represented by two equivalent sources, the minimum needed to discern an extended region of correlated magnetization. The large amplitude ratio and small cap half angle on the bottom line of Table 2 are artifacts of carrying LPM to excessive degrees. Similar artifacts can be found by fitting damped spectra.

[74] Does this mean that magnetization models underlying LPM or damped spectra are bad? No. The measured data do not uniquely determine Mars' magnetization, but they do constrain it. Either omission of fine-scale structure or suppression of magnetization or in hopes of making a more helpful broad-scale map are not unreasonable. But this neither implies nor suggests that there is little or no narrower-scale magnetization. The fact that small-scale fields are required to adequately fit available low-altitude data [*Cain et al.*, 2003] tells us that small-scale magnetization is present. The data may not resolve this fine structure everywhere, but it can still constrain the spectrum. Either omission of, or appreciable misfit to, key data can corrupt a magnetic spectrum as surely as downward continuation of poorly determined phase information can corrupt a magnetic map.

7. Comparisons and Inferences

[75] Typical source depth $z = 23.9 \pm 4.2$ km is doubled to put the typical magnetic crustal thickness of Mars at 47.8 ± 8.4 km. How does this compare with other values, and with values for geochemical, geodetic, or rheologic crustal thicknesses? Because characteristic half angle, $\psi^* = 5.48 \pm 0.21°$, is large and amplitude ratio, $B_v/A_v = 1.63 \pm 0.34$, exceeds unity, the extended sources are enormous, typically 11° or 650 km across, and account for over half the magnetic energy at low degree. Are there other signs of such vast sources? If so, how did they form?

7.1. Magnetic and Other Crustal Thicknesses

[76] *Connerney et al.* [1999] model intense linear magnetic features in low-altitude AB passes with cross-track magnetized strips. They assume a 30 km depth so as to plot magnetization (A/m) instead of magnetization-times-thickness. *Arkani-Hamed* [2002a] uses a nominal magnetic thickness of 50 km. *Whaler and Purucker* [2005] specify a magnetic layer thickness of 40 km. These assumed thicknesses are fairly close to the present magneto-spectral estimate.

[77] This estimate includes the center of the 10–100 km magnetic layer thickness range that *Nimmo and Gilmore* [2001] obtain for impact demagnetization and is but slightly thicker than their nominal value of 30–40 km. This depends upon assumptions about effects of giant impacts. *Langlais et al.* [2004] examined residuals as a function of equivalent

source shell radius at 10 km steps before selecting 3373.5 km. The corresponding shell depth, about 16 ± 5 km here, can depend on assumed source spacing, yet is only slightly less than the present estimate (23.4 ± 4.2 km).

[78] *Neumann et al.* [2004] use MGS tracking and Mars Orbiter Laser Altimeter (MOLA) data to construct a gravito-topographic map of the thickness of Mars' geodetic crust. With neither seismologic estimates nor direct measurements of Mars' crustal thickness, they must assume a mean crust-mantle interface depth. They cite: geochemical arguments for a mean thickness in the range of 100–250 km, yet an enriched geochemical crustal thickness of less than 45 km; viscous relaxation arguments for a 50–100 km rheologic thickness; and combined physical and chemical arguments for a 50 km crustal thickness. They choose a mean geodetic crustal thickness of 45 km, in excellent agreement with the magneto-spectral estimate.

[79] *Arkani-Hamed* [2005] uses thermal evolution modeling to obtain some possible upper limits on Curie isotherm depths, hence maximal magnetic crustal thicknesses. For pyrrhotite, magnetite, or hematite, these limits are 45–55 km, 80–90 km, or 90–100 km, respectively. In addition to several restrictions on a one dimensional parameterized thermal history model, however, these limits depend upon assumed values for nine varied parameters (initial crustal thickness, viscosity activation energy, initial temperature, core super heat, uranium content, radioactivity model, fraction of radionuclides in the crust, fraction of potassium in the core, and thermal expansion coefficient). These limits are indeed at or above the present estimate for thickness of Mars' magnetic crust, which depends upon the simple supposition that Mars contains both compact and extend magnetic sources near the middepth of a magnetized layer.

[80] *Ruiz et al.* [2006] try a different approach to modeling possible Curie isotherm depths. The model results depend upon trial values assumed for many parameters, notably for the thickness of a radioactive element rich crust and the fraction of surface heat flow from it. They specify layer temperature as a function of depth in terms of surface heat flux, thermal conductivity (assumed that of diabase), a boundary temperature, and the two radiocrustal parameters. Next, functions are identified that relate effective elastic thickness and topographic curvature to plate bending moment, and bending moment to the vertical integral through a mechanical lithosphere of an offset depth weighted, temperature-dependent, lithospheric strength envelope. This integral depends upon formulas used to calculate the brittle strength, temperature-dependent ductile strength (which also assumes diabase and a slow strain rate), and fiber stress, as well as a depth to a neutral stress plane. With temperature profile, hence strength envelope, expressed in terms of thermal parameters, one parameter may in principle be computed from trial values for the others. *Ruiz et al.* [2006] compute surface heat flux from elastic thickness, curvature, boundary temperature, fraction of surface heat flow from a radioactive crust, and thickness of that crust, plus parameters used in the strength integral. This surface heat flux is then used to recover a temperature profile. Sample calculations by *Ruiz et al.* [2006] intended for Terra Cimmeria, in the western part of the southern magnetic province, give Curie depths of less than 20 km for pyrrhotite; 32–35 km, 41–48 km, or more for magnetite; and 37–40 km or more for hematite. It is thought that the present, comparatively direct, estimate for the typical thickness of Mars' magnetic crust might help constrain some combination of the many thermal, compositional, and rheologic parameters appearing in such formulations.

[81] Arguments about crustal thicknesses based on assumed depths or meshes; assumed upscaling of laboratory and field shock data to giant impacts, target properties and magnetic mineralogy; assumed chemical compositions; assumed initial and boundary conditions for thermal histories; assumed density contrasts; and/or assumed rheology and material properties are outside the focus of this paper. The present estimate of magnetic crustal thickness makes no such assumptions. It depends only on the magnetic spectrum of Mars and a simple statistical treatment of both compact and extended magnetic sources.

[82] It is remarkable that such arguments and assumptions yield various crustal thicknesses close to the magneto-spectral estimate. The agreement offers considerable support for those assumptions, but care is needed in detailed comparisons. For example, a nominal 35 ± 5 km paleothickness from *Nimmo and Gilmore* [2001] would not include magnetization of deeper rock by overlying sources as the Curie isotherm propagates into the cooling planet, and so may suggest 13 ± 10 km of magnetic crustal thickening rather than a flaw in an impact demagnetization model. Lithospheric thicknesses depend on rheology and loading rather than magnetic history and mineralogy. Moreover, typical magnetic crustal thickness need not represent large portions of Mars that appear nonmagnetic at MGS altitudes [*Acuña et al.*, 1999]. The agreement of the magneto-spectral estimate with the mean geodetic crustal thickness of *Neumann et al.* [2004] implies that weakly or nonmagnetic crust that is geodetically thick (Tharsis) can compensate for that which is geodetically thin (Hellas, Argyre, Isidis and portions of the northern lowlands).

7.2. Vast Source Regions

[83] There are signs of these regions in the magnetic phase information. The map by *Acuña et al.* [1999, Figure 2] reveals a complex magnetic province over the southern highlands from about 10°S to 85°S latitude and 145°E to 235°E longitude; the most intense fields are south of 30°S. *Connerney et al.* [1999, Figure 1] show a prominent, east-west trending, positive radial magnetic feature in this province, near (53°S, 180°E), that can be followed over 2000 km and nearby, quasi-parallel features that can be traced for 1000 km. This feature spans up to 12° of latitude; another up to 15° (>2ψ*). Six peaks in $|B_z|$ in one 2700 km along-track segment (Connerney et al.'s Figure 2) suggest a scale of roughly 450 km, but fits with magnetized strips 200 km along track (Connerney et al.'s Figures 2–5) show up to 5 adjacent strips, hence a 1,000 km wide band, of like vertical polarity.

[84] Over the southern subprovince, from about 35°S to 80°S and about 150°E to 220°E, the map by *Purucker et al.* [2000, Plate 1] shows 5 salient bands of intense B_r, with a mean latitudinal extent of about 9°(<2ψ*). The midsection of the northern negative B_r band extends northward, separating two huge, irregular patches of positive B_r from 35°S to 10°S. Maps by *Connerney et al.* [2001, Figure 1 and cover plate] show these bands and patches in B_r, bands in

B_θ, and patches in B_φ. Similar features are evident in maps by *Arkani-Hamed* [2002a, Figure 2; 2004, Figure 6], *Langlais et al.* [2004, Figure 4], *Whaler and Purucker* [2005, Figure 1], and others. Along-track first differences in B_r mapped by *Connerney et al.* [2005] show 6 zones of steep gradient in the southern subprovince: the 5 arcs of zero gradient trace crest or trough lines of the 5 bands.

[85] Many lesser magnetic features appear in all these maps. Indeed, within the area (10°S to 80°S, 150°E to 220°E), the map by *Purucker et al.* [2000] shows at least 32 extrema in B_r. With at least 7, and perhaps 32 or more, magnetic features over this 11.4×10^6 km^2 area, mapped features average from at most 1.6×10^6 km^2 to 350,000 km^2 or less. Because a simple source region can cover far less area than features in its fringing field at satellite altitude, correlated source areas of order 10^5 to 10^6 km^2 are quite plausible. Such a source may, however, create features of different polarity, so one-to-one correspondence between features and source regions is not assured, particularly in a complex magnetic province.

[86] Evidently, spectral signatures of the intense magnetic bands and patches drives the estimated typical cap diameter up to 11°, cap area to 330,000 km^2, and amplitude ratio to well above unity. These estimates are reasonable enough to lend some support to the estimate of z.

[87] Vector magnetization models preferred by *Langlais et al.* [2004], *Whaler and Purucker* [2005], and *Chiao et al.* [2006] do show extensive, irregular patches of laterally correlated magnetization in the southern hemisphere around 180° longitude, as well as myriad smaller structures. But there is another category of magnetization models.

[88] M. Acuña (personal communications, 2002, 2006) points out that key features of the measured field may instead be the fringing field from smaller gaps or holes in a slab of permeable, horizontally magnetized crust, gaps filled with virtually nonmagnetic material. Narrow gaps or fractures could be made by faults, or perhaps dikes or rifts, radiating from Tharsis; holes could be made by impacts; and the fringing field above a hole would be much like that of a horizontally magnetized cap, with a spectrum akin to (12b). Yet this elegant model presupposes a far larger slab of magnetized crust. Indeed, if most or all the salient magnetic bands and patches come from gaps and holes in one slab of correlated magnetization, then that slab is the size of the entire magnetic province, about 35 times the typical cap area. In this light, 330,000 km^2 can be seen as a least upper bound on the area of slabs of correlated magnetization in Mars.

[89] Magneto-spectral analysis, field morphology, and either detailed magnetization or demagnetization models, thus lead to the same general conclusion. Some features in the measured field come from vast regions of laterally correlated magnetization in Mars' crust.

7.3. How Could Such Regions Form?

[90] Formation and magnetization of the entire highland magnetic province during a single polarity chron of a paleodipolar core source field, via bulk cooling and TRM of a compositionally buoyant chill crust, would be enough to provide the magnetized slab needed for subsequent fracture and puncture in the Acuña model. The broad range of paleodipole latitudes spanned by such a protoprovince merely suggests some deviations from horizontal magnetization. There are, however, other models, other magnetic provinces, and indications of reversals. So here we address the formation question via the present estimate of source size.

[91] The regions in question are slabs of roughly uniformly magnetized crust, typically about 650 km across, 330,000 km^2 in area, 48 km thick, and 1.6×10^7 km^3 in volume. The simplest way for remnant magnetization to become strongly correlated throughout such a volume is for each region to form during a single polarity chron of an ancient core source dipole field.

[92] In fact, eligible formation mechanisms only need to eventually magnetize such area and depth. Some fraction of the depth may be accounted for by propagation of the Curie isotherm into the planet (see Appendix A), or perhaps a serpentinization front (L. Hood, personal communication, 2006). For this fraction to be appreciable, an initial seed layer must have enough vertically integrated vertical magnetization to bias the polarity of the entire volume, enough to offset any tendency for subsequent reversals to produce a stack of alternating polarity layers with little vertically integrated magnetization. This condition is more easily met by a seed layer magnetized during the final chron. Intermittent formation is also conceivable, but appeals to coincidence of active episodes with chrons of one polarity.

[93] Apart from these special exceptions, each region arguably formed during a single polarity chron. The typical formation time is thus taken as less than or equal to a typical chron duration. Can we see signs of polarity chrons? If so, how many, or how few? How long did they last?

[94] The models of *Connerney et al.* [1999] show 6 to 11 changes in the sign of the vertical magnetization component of cross-track strips, depending on the pass. This suggests up to 12 chrons (6 at two strips per chron). My initial guess of 12 polarity transitions in at most 0.3 Ga, hence a mean duration for "visible chrons" of up to 25 Ma, is not good enough. There are 8 to 13 changes in the sign of B_r over this subprovince, depending on the pass, which admits 7 to 12 adjacent vertically magnetized strips of alternating polarity. A pass crossing J well separated vertically magnetized strips, however, could show $3J$-1 changes in sgn(B_r) if strips alternate polarity ($2J$ if all are upwardly magnetized). The 13 count thus admits as few as 5 source strips, and only if each formed during a different chron were there at least 5 chrons.

[95] My counts across the global first difference map by *Connerney at al.* [2005] give up to 17 main east-west bands, hence as many as 18 main chrons, but there are many other features. At high latitude, the cylindrical equidistant map projection stretches patches into east-west bands and bands into east-west strips. Yet the map clearly shows extensive east-west bands at low latitudes. Some features at different locations might have formed during the same chron, yet finer resolution maps from lower altitude data may well reveal far more features.

[96] Core dynamo action in Mars is thought to have started with core formation about 4.5 billion Earth years (Ga) ago and stopped before impact demagnetization around Hellas and Argyre basins. These basin floors do not appear to have been remagnetized, though signals from many layers of alternating polarity could be hard to detect at

MGS altitudes. If these basins formed near the time of large lunar impact basins about 3.8 Ga ago, then Mars' core dynamo operated for about 0.7 Ga. Yet *Acuña et al.* [2001] cite age estimates of <0.3 Ga.

[97] Granted only 5 to 18 "visible chrons" in a core dynamo life of 250 to 750 Ma, these chrons of Mars were of order 15 to 150 Ma long, comparable to Earth's superchrons. Terrestrial experience indicates that lower altitude satellite, balloon, or aeromagnetic data, if not oriented subsurface samples, are needed to discover if shorter chrons are recorded in the crust of Mars.

[98] In such a superchron, a magnetic region could form via several endogenic processes. Perhaps the most likely are igneous processes with TRM acquisition: bulk cooling of an initial crust; extrusive overplating by laminated lava flows which thicken into a subsiding volcanic cap or shield; intrusion by iron rich swarms of dikes and sills; spreading of new crust away from a rift during an era of more active mantle convection; or some combination of these.

[99] Whether or not 15–150 Ma is enough time to cool the bulk of a 48 km thick slab of hot young Martian crust below its Curie point via conduction and hydrothermal circulation is not clear: porosity might be high in rock compressed only by Mars' low gravity, but initial conditions are uncertain. Either way, to magnetize one region this way while another awaits a different chron demands laterally heterogeneous cooling. To form several such regions within one province would seem to require heterogeneous preheating, which amounts to a different mechanism. Lateral accretion of many different magnetized regions, however, offers an alternative to bulk cooling of an entire highland magnetic protoprovince during a single chron.

[100] A sequence of thin, extrusive lava flows, each cooling by radiation and convection to and through an early atmosphere, could accumulate tens of km of thickness in 15 to 150 Ma. Indeed, solidification of lava and TRM acquisition a rate of but 3.2 to 0.32 mm/a would overplate a thin protocrust with a 48 km thick layer in 15 to 150 Ma. Eruption rates as low as 1 to 0.1 km^3/a scattered over a 330,000 km^2 region would fill the requisite volume in this interval. Such rates seem modest for a planet which formed the Tharsis volcanic province. In this way, different magnetized regions could form during different chrons, either as different magma sources arose, or as one (or more) magma source(s) translated relative to the crust. Sufficiently precise relative dating techniques could either offer support for such differential overplating, or force igneous activity underground, to intrusive dikes and sills.

[101] Repeated dike intrusions are a possible cause of magnetic lineations in the southern magnetic province [*Nimmo*, 2000] and magnetic features elsewhere. Though some source regions might be magnetized extrusive layers, perhaps even some portions of the southern province where impacts have largely erased older surface features, extrusives must be supplied by magma conduits and/or feeder dikes. Not all the latter need erupt; those which do eventually stop. A detailed igneous formation mechanism for thick, New Mexico sized regions of magnetic crust must thus include intrusives. Formation intervals of up to 15–150 Ma allow ample time for even large units to cool and acquire TRM. Large volumes of intruded material can also help explain uplift in the southern highland magnetic province. Moreover, the heat of intruding magma can drive hydrothermal circulation in nearby crust. This may not only produce enough water to erode valley networks [*Harrison and Grimm*, 2002], but may supplement TRM with CRM and so help explain large inferred intensities for Mars' crustal magnetization.

[102] One candidate nonigneous endogenic formation process for such a region is depositional remnant magnetization (DRM) of exceptionally magnetic, fine grained aeolian, if not subaqueous, sediments in a large basin. Ancient deposition rates of 3 to 0.3 mm/a seem plausible; however, even granting a huge source of magnetic fines, it is hard to see how to accommodate or drive 48 km of basin subsidence. It is perhaps still harder to see how many such basins could either form nearby or accrete, and then be uplifted to become part of the highlands without appreciable demagnetization of soft DRM. Another endogenic process, chemical remnant magnetization (CRM) acquired under putative paleolakes or seas, might conceivably penetrate to such depth. There would again be a need for uplift without demagnetization for the highland province, so this type of CRM, and perhaps chemical demagnetization, would also seem more likely to be found under basins.

[103] Exogenic processes can also cover large areas and fill great depth. Though visible impact craters are associated with excavation rather than regional fill, Mars' accretion arguably involved a rapid sequence of a great many impacts that increased the volume of the growing planet. Indeed, a very early crust might amount to layer upon layer of backfilled impact basins. Impact melts and ejecta can cover large areas and acquire TRM on cooling; however, it is hard to see how self-compacting regolith could attain great thickness in one region, then be preserved with unaltered magnetization while a similar region formed nearby during another chron. Impact release of underlying magma seems more plausible, and might start an epoch of regional igneous activity. In light of the contrast between lunar mare and highlands, however, the problem of subsequent uplift without demagnetization arises again. A third candidate exogenic process is shock induced magnetization and remagnetization (akin to hammering a steel needle). This seems more likely to randomly magnetize scattered irons than to coherently magnetize a New Mexico sized target region.

8. Summary

[104] To estimate the thickness of the magnetic crust of Mars, six different observational magnetic spectra were analyzed in terms of a novel, bimodal distribution of magnetic sources. Each spectrum represents the mean square magnetic induction configured in spherical harmonics of degree n, averaged over a sphere containing the magnetic sources inside Mars. Such spectra differ, for each comes from a different published map or model of variously selected MGS-MAG/ER measurements of the vector magnetic field around Mars. Observational spectra were fitted with a theoretical magnetic spectrum that represents contributions from both compact magnetized bodies and extended regions of laterally correlated magnetization. This spectrum is derived from a simple statistical model of such complex sources. The model has both uncorrelated vertical

dipoles of random polarity scattered on a spherical shell, and an independent ensemble of uncorrelated, homogeneously and vertically magnetized spherical caps, also of random polarity, on the same shell. The four spectral parameters estimated give: source shell depth z, regarded as half the typical thickness of Mars' magnetic crust; cap half angle ψ^*, hence the typical breadth and area of extended sources; amplitude for compact sources A_v; and relative amplitude for extended sources B_v/A_v.

[105] For all observational spectra and all degree ranges analyzed, this bimodal source distribution gives a better fit than do compact sources alone. Only by paying careful attention to points made by various authorities, however, can the physically useful maximum and minimum degrees of each observational spectrum be determined. By fitting each spectrum within its recommended degree range, one learns about Mars. Outside the recommended range, one learns about the limitations of various data subsets and analysis techniques.

[106] Source shell depth is about half the decorrelation depth, as anticipated. Extended sources are enormous, typically 650 km across, and account for over half the magnetic energy at low degrees. The mean of all shell depth estimates is 22 km below the sphere of radius 3389.5 km. Most of the scatter comes from one spectrum, which suggests depths of but 7 km and may arguably indicate that extended source regions are relatively shallow. Outliers were nonetheless excluded to put the typical source depth at $z = 23.9 \pm 4.2$ km. The uncertainty is between formal estimation errors, which are too small, and unscaled errors, which are too large. The result for the typical thickness of the magnetic crust of Mars is 47.8 +/− 8.4 km.

[107] This magneto-spectral estimate agrees fairly well with other values found in the literature: magnetic, geochemical, geodetic, and rheologic thicknesses based on assumed depths; assumed upscaling of laboratory and terrestrial field shock data to giant impacts, target properties and magnetic mineralogy; assumed chemical composition; assumed initial and boundary conditions for thermal histories; assumed density contrasts; or assumed rheology and material properties. The agreement offers some validation for those assumptions, bearing in mind that the magneto-spectral estimate uses a simplified statistical treatment of Mars' magnetic crust, a nonuniform crust which may have thickened somewhat over eons.

[108] The typical breadth and area of the extended sources are estimated to be 650 km and 330,000 km^2, respectively, about the size of the State of New Mexico. Of course, some source regions will be smaller and others larger. Indeed, phase information in magnetic maps suggests areas of 10^5 to 10^6 km^2 are quite plausible. But there are vast regions of laterally correlated magnetization in Mars' crust. This poses a fundamental geophysical and areologic question: how did such vast regions of roughly uniformly magnetized crust form?

[109] From many plausible answers, one correct answer to this question cannot yet be selected. Indeed, there may be no single answer, for different source regions in different magnetic provinces may have different origins. Apart from a few special exceptions, however, each such region arguably formed during a single polarity chron of a paleodipolar core source field.

[110] Efforts to reckon the number of chrons and the interval of core dynamo action gave a soft upper bound on mean chron duration of order 15 to 150 Ma, comparable to a terrestrial superchron, the only ones large enough to detect from high orbit. The corresponding soft lower bounds on layer accumulation and volumetric formation rates for a typical extended source region are 3 to 0.3 mm/a and 1 to 0.1 km^3/a, respectively. These rates do not constrain all eligible mechanisms, but are low enough to keep paleo-igneous activity high on the list of viable formation mechanisms for such regions, each of which is much smaller than Tharsis.

Appendix A: A Conceptual Model

[111] As early Mars cooled, thermal convection stirred its fluid, iron-rich core to motion at nonuniform fluid velocity **v**. Motion of the fluid conductor across a nonuniform magnetic field of flux density **B** caused electromotive force $\mathbf{v} \times \mathbf{B}$. This drove electric current of density **J** by Ohm's law, and changed the field by Faraday induction, perhaps causing a once largely dipolar field on Mars' surface to reverse many times, much as has Earth's. Electric resistance to the source current also changed the ancient core field via magnetic diffusion. Core flow was complicated spatially and likely unsteady due to an imbalance between gravitational, pressure, Lorentz ($\mathbf{J} \times \mathbf{B}$), and viscous forces on the one hand, and centrifugal, Coriolis, Poincare, and advective effects on the other. Yet fluid motions that curled the field against opposing Lorentz forces drove electric currents which, in turn, acted as sources for the field itself. According to dynamo theory, the conversion of kinetic energy in such motions into magnetic energy replaced the magnetic energy converted to heat via Ohmic dissipation of the source currents. This maintained a core field for a fraction of areologic time. As Mars lost heat, however, its congealing viscoelastic mantle could no longer remove the remaining core heat fast enough. Core convection slowed and stopped; the currents decayed, and its core field diffused away.

[112] Before the core field died, igneous rock cooling in it acquired hard thermoremanent magnetization (TRM). Chemical reactions, notably serpentinization (K. Nazarova, personal communication, 1999), may also have created minerals that acquired chemical remanent magnetization (CRM). Though vast regions were later demagnetized by the shock of giant meteor impacts, and other areas were altered by chemical, metamorphic and volcanic processes, much of Mars' crust retains its ancient magnetization. This crust is far more intensely magnetized than Earth's, in part due to the abundance of iron-rich magnetic minerals in the red planet. And so, as the Curie isotherm propagates deeper into the slowing cooling planet, rock at depth may still be magnetized in the field from the overlying crust.

[113] Of course, the field from a vertically magnetized block imposes a parallel field upon the rock just below it. So newly acquired TRM (and CRM) at depth increases depth-integrated vertical magnetization. But the fringing field from a horizontally magnetized block imposes an anti-parallel horizontal field on the rock below. So newly acquired remanence at depth decreases depth-integrated horizontal magnetization. When integrated throughout a slowly thickening magnetic crust, this effect tends to amplify absolute

vertical magnetization and weaken absolute horizontal magnetization. It also suggests a modern magnetic crust somewhat thicker than the ancient crust. The process also tends to make surface magnetic inclination steeper with time. One may thus expect high paleolatitudes to be somewhat more common on Mars than indicated by a reversible centered dipolar field. How much this effect contributes to models of vector magnetization and paleopole positions is unknown.

[114] This thickening of magnetic crust has already be simulated by *Arkani-Hamed* [2003], who previously studied it in Earth's oceanic crust. In some Mars-like scenarios, the vertically integrated vertical magnetization can almost double over time (J. Arkani-Hamed, personal communication, 2006); however, the additional contribution to measurable magnetic anomalies is attenuated by the greater depth of the newly magnetized material. In contrast, signals from detrital remanent magnetization (DRM) acquired by aeolian fines rich in iron oxides (and perhaps ejecta, if not subaqueous sediments), deposited atop previously magnetized crust do not suffer such additional attenuation. There are many terrestrial examples of thick sedimentary deposits which have been metamorphosed and uplifted, but it is not clear that DRM acquired on Mars contributes much to the measured field.

[115] **Acknowledgments.** Special thanks to M. Acuña, J. Connerney, H. Frey, M. Purucker, J. Heirtzler, J. Cain, J. Arkani-Hamed, B. Langlais, G. Kleteschka, W. Kuang, T. Sabaka, F. Nimmo, and two anonymous referees for coefficients, spectra, insightful discussions, and helpful comments. My thanks to the people of the United States who supported this work via NASA's Mars Data Analysis Program, MDAP03-000-008.

References

Acuña, M. H., et al. (1999), Global distribution of crustal magnetization discovered by Mars Global Surveyor MAG/ER experiment, *Science*, *284*, 790–793, doi:10.1126/science.284.5415.790.

Acuña, M. H., et al. (2001), Magnetic field of Mars: Summary of results from aerobraking and mapping orbits, *J. Geophys. Res.*, *106*(E10), 23,403–23,417, doi:10.1029/2000JE001404.

Arkani-Hamed, J. (2001a), Paleomagnetic pole positions and pole reversals of Mars, *Geophys. Res. Lett.*, *28*(17), 3409–3412, doi:10.1029/2001GL012928.

Arkani-Hamed, J. (2001b), A degree 50 spherical harmonic model of the magnetic field of Mars, *J. Geophys. Res.*, *106*(E10), 23,197–23,208, doi:10.1029/2000JE001365.

Arkani-Hamed, J. (2002a), Magnetization of the Martian crust, *J. Geophys. Res.*, *107*(E5), 5032, doi:10.1029/2001JE001496.

Arkani-Hamed, J. (2002b), An improved 50-degree spherical harmonic model of the magnetic field of Mars derived from both high-altitude and low-altitude data, *J. Geophys. Res.*, *107*(E10), 5083, doi:10.1029/2001JE001835.

Arkani-Hamed, J. (2003), Thermoremanent magnetization of the Martian lithosphere, *J. Geophys. Res.*, *108*(E10), 5114, doi:10.1029/2003JE002049.

Arkani-Hamed, J. (2004), A coherent model of the crustal magnetic field of Mars, *J. Geophys. Res.*, *109*, E09005, doi:10.1029/2004JE002265.

Arkani-Hamed, J. (2005), Magnetic crust of Mars, *J. Geophys. Res.*, *110*, E08005, doi:10.1029/2004JE002397.

Arkani-Hamed, J., R. Langel, and M. Purucker (1994), A magnetic anomaly map of the Earth derived from POGO and Magsat data, *J. Geophys. Res.*, *99*(B12), 24,075–24,090, doi:10.1029/94JB00930.

Artemieva, N., L. Hood, and B. A. Ivanov (2005), Impact demagnetization of the Martian crust: Primaries versus secondaries, *Geophys. Res. Lett.*, *32*, L22204, doi:10.1029/2005GL024385.

Cain, J. C., S. J. Hendricks, R. A. Langel, and W. V. Hudson (1967), A proposed model for the International Geomagnetic Reference Field—1965, *J. Geomagn. Geoelectr.*, *19*, 335–355.

Cain, J. C., Z. Wang, and D. R. Schmitz (1989), Derivation of a geomagnetic field model to n = 63, *Geophys. J.*, *97*, 431–441.

Cain, J. C., B. B. Ferguson, and D. Mozzoni (2003), An n = 90 internal potential function of the Martian crustal magnetic field, *J. Geophys. Res.*, *108*(E2), 5008, doi:10.1029/2000JE001487.

Chiao, L.-Y., J.-R. Lin, and Y.-C. Gung (2006), Crustal magnetization equivalent source model of Mars constructed from a hierarchical multiresolution inversion of the Mars Global Surveyor data, *J. Geophys. Res.*, *111*, E12010, doi:10.1029/2006JE002725.

Connerney, J., M. Acuña, P. Wasilewski, N. Ness, H. Rème, C. Mazelle, D. Vignes, R. Lin, D. Mitchell, and P. Cloutier (1999), Magnetic lineations in the ancient crust of Mars, *Science*, *284*, 794–798, doi:10.1126/science.284.5415.794.

Connerney, J. E. P., M. H. Acuña, P. J. Wasilewski, G. Kletetschka, N. F. Ness, H. Rème, R. P. Lin, and D. L. Mitchell (2001), The global magnetic field of Mars and implications for crustal evolution, *Geophys. Res. Lett.*, *28*, 4015–4018, doi:10.1029/2001GL013619.

Connerney, J. E. P., M. H. Acuña, N. F. Ness, G. Kletetschka, D. L. Mithcell, R. P. Lin, and H. Reme (2005), Tectonic implications of Mars crustal magnetism, *Proc. Natl Acad. Sci. U.S.A.*, *102*(42), 14,970–14,975, doi:10.1073/pnas.0507469102.

Curtis, S. A., and N. F. Ness (1988), Remanent magnetism at Mars, *Geophys. Res. Lett.*, *15*, 737–739, doi:10.1029/GL015i008p00737.

Dunlop, D. J., and G. Kletetschka (2001), Multidomain hematite: A source of planetary magnetic anomalies?, *Geophys. Res. Lett.*, *28*(17), 3345–3348.

Frawley, J. J., and P. T. Taylor (2004), Paleo-pole positions from Martian magnetic anomaly data, *Icarus*, *172*, 316–327, doi:10.1016/j.icarus.2004.07.025.

Harrison, K. P., and R. E. Grimm (2002), Controls on Martian hydrothermal systems: Application to valley network and magnetic anomaly formation, *J. Geophys. Res.*, *107*(E5), 5025, doi:10.1029/2001JE001616.

Hood, L., and A. Zakharian (2001), Mapping and modeling of magnetic anomalies in the northern polar region of Mars, *J. Geophys. Res.*, *106*, 14,601–14,619, doi:10.1029/2000JE001304.

Hood, L. L., N. C. Richmond, E. Pierazzo, and P. Rochette (2003), Distribution of crustal magnetic fields on Mars: Shock effects of basin-forming impacts, *Geophys. Res. Lett.*, *30*(6), 1281, doi:10.1029/2002GL016657.

Hood, L. L., C. N. Young, N. C. Richmond, and K. P. Harrison (2005), Modeling of major Martian magnetic anomalies: Further evidence for polar reorientations during the Noachian, *Icarus*, *177*, 144–173, doi:10.1016/j.icarus.2005.02.008.

Kletetschka, G., P. J. Wasilewski, and P. T. Taylor (2000), Mineralogy of the sources for magnetic anomalies on Mars, *Meteorit. Planet. Sci.*, *35*(5), 895–899.

Kletetschka, G., J. E. P. Connerney, P. J. Wasilewski, and M. Acuña (2002), Shock demagnetization of Martian crust, *Eos Trans. AGU*, *83*(19), Spring Meet. Suppl., Abstract P32A-04.

LaBrecque, J. L., and C. A. Raymond (1985), Seafloor spreading anomalies in the Magsat field of the North Atlantic, *J. Geophys. Res.*, *78*, 2565–2575.

Langel, R. A. (1987), The main field, in *Geomagnetism*, vol.1, edited by J. A. Jacobs. pp. 249–512, Academic, Orlando, Fla.

Langel, R., and R. Estes (1982), A geomagnetic field spectrum, *Geophys. Res. Lett.*, *9*, 250–253, doi:10.1029/GL009i004p00250.

Langlais, B., M. E. Purucker, and M. Mandea (2004), Crustal magnetic field of Mars, *J. Geophys. Res.*, *109*, E02008, doi:10.1029/2003JE002048.

Lowes, F. J. (1966), Mean-square values on sphere of spherical harmonic vector fields, *J. Geophys. Res.*, *71*(8), 2179.

Mauersberger, P. (1956), Das Mittel der Energiedichte des geomagnetischen Hauptfeldes der Erdoberfläche und seine säkulare Änderung, *Gerlands Beitr. Geophys.*, *65*, 207–215.

Neumann, G. A., M. T. Zuber, M. A. Wieczorek, P. J. McGovern, F. G. Lemoine, and D. E. Smith (2004), Crustal structure of Mars from gravity and topography, *J. Geophys. Res.*, *109*, E08002, doi:10.1029/2004JE002262.

Nimmo, F. (2000), Dike intrusion as a possible cause of linear Martian magnetic anomalies, *Geology*, *28*, 391–395, doi:10.1130/0091-7613(2000)28<391:DIAAPC>2.0.CO;2.

Nimmo, F., and M. S. Gilmore (2001), Constraints on the depth of magnetized crust on Mars from impact craters, *J. Geophys. Res.*, *106*(E6), 12,315–12,323, doi:10.1029/2000JE001325.

Purucker, M. E., and J. Dymet (2000), Satellite magnetic anomalies related to seafloor spreading in the South Atlantic ocean, *Geophys. Res. Lett.*, *27*, 2765–2768, doi:10.1029/1999GL008437.

Purucker, M., D. Ravat, H. Frey, C. Voorhies, T. Sabaka, and M. Acuña (2000), An altitude-normalized magnetic map of Mars, *Geophys. Res. Lett.*, *27*, 2449–2452, doi:10.1029/2000GL000072.

Ravat, D. (2006), Uncertainty in magnetization directions derived from planetary magnetic anomalies in view of numerical experiments with coalesced anomalies from Earth, *Eos Trans. AGU*, *87*(52), Fall Meet. Suppl., Abstract GP11B-0076.

Richmond, N., and L. Hood (2002), Mapping and modeling of major Martian magnetic anomalies, *Eos Trans. AGU*, *83*(19), Spring Meet. Suppl., Abstract GP41A-07.

Rochette, P., G. Fillion, R. Ballou, F. Brunet, B. Ouladdiaf, and L. Hood (2003), High pressure magnetic transition in pyrrhotite and impact demagnetization on Mars, *Geophys. Res. Lett.*, *30*(13), 1683, doi:10.1029/2003GL017359.

Ruiz, J., P. J. McGovern, and R. Tejero (2006), The early thermal and magnetic state of the cratered highlands of Mars, *Earth Planet. Sci. Lett.*, *241*, 2–10, doi:10.1016/j.epsl.2005.10.016.

Sabaka, T. J., N. Olsen, and M. E. Purucker (2004), Extending comprehensive models of the Earth's magnetic field with Oersted and CHAMP data, *Geophys. J. Int.*, *159*, 521–547, doi:10.1111/j.1365-246X.2004.02421.x.

Thomas, H. H. (1987), A model of ocean basin crustal magnetization appropriate for satellite elevation anomalies, *J. Geophys. Res.*, *92*, 11,609–11,613, doi:10.1029/JB092iB11p11609.

Voorhies, C. V. (1998), Elementary theoretical forms for the spatial power spectrum of Earth's crustal magnetic field, *NASA Tech. Pap. 1998-208608,* 38 pp., Dec.

Voorhies, C. V. (2004), Narrow-scale flow and a weak field by the top of Earth's core: Evidence from Ørsted, Magsat and secular variation, *J. Geophys. Res.*, *109*, B03106, doi:10.1029/2003JB002833. (Correction, *J. Geophys. Res., 109*, B08103, doi:10.1029/2004JB003289, 2004.)

Voorhies, C. V. (2006), A geomagnetic estimate of mean paleointensity, *J. Geophys. Res.*, *111*, B11105, doi:10.1029/2005JB003874.

Voorhies, C. V., T. J. Sabaka, and M. Purucker (2002), On magnetic spectra of Earth and Mars, *J. Geophys. Res.*, *107*(E6), 5034, doi:10.1029/2001JE001534.

Whaler, K. A., and M. E. Purucker (2005), A spatially continuous magnetization model for Mars, *J. Geophys. Res.*, *110*, E09001, doi:10.1029/2004JE002393.

C. V. Voorhies, Planetary Geodynamics Laboratory, Goddard Space Flight Center, Mail Code 698, Building 33, Room F362, Greenbelt, MD 20771, USA. (coerte.v.voorhies@nasa.gov)